Edelweiss Applied Science and Technology
ISSN: 2576-8484
Vol. 9, No. 3, 1692-1704
2025
Publisher: Learning Gate
DOI: 10.55214/25768484.v9i3.5680
© 2025 by the authors; licensee Learning Gate

Research on the method of measuring blasting stress waves in water-filled boreholes

Duc Ngo The[1*], Thang Dam Trong[2], Thuy Ngo Ngoc[3]
[1,2,3]Institute of Technical for Special Engineering Le Quy Don Technical University, 236 Hoang Quoc Viet, Hanoi, Vietnam, 100000; ducnt1988@lqdtu.edu.vn (D.N.T.) thangdt@lqdtu.edu.vn (T.D.T.) ngocthuy.ngo@lqdtu.edu.vn (T.N.N.)

Abstract: Accurately measuring stress waves generated during blasting is crucial for understanding rock failure mechanics. Traditional methods rely on large water-filled pits for measurement, which are costly and impractical for small-scale experiments. This study introduces a novel approach using water pressure sensors in small-diameter (14 mm) boreholes, providing a cost-effective and scalable alternative. Numerical simulations and experimental tests were conducted to validate this method. A conversion coefficient of 0.598 was derived to translate borehole measurement results into equivalent values for water-filled pits, accounting for borehole geometry effects on wave transmission. Advanced material models, including the Holmquist-Johnson-Cook model for concrete and the Jones-Wilkins-Lee equation for TNT, were used to simulate wave propagation accurately. Experiments using coral concrete blocks and 1 g TNT charges confirmed the reliability of this approach, with a margin of error of approximately 5% between simulation and experimental results. The findings highlight a practical and precise method for measuring transmitted stress waves in rock formations. This method not only improves measurement accuracy but also significantly reduces costs associated with stress wave analysis in blasting, making it particularly suitable for small-scale geotechnical applications.

Keywords: *Blasting stress waves, Explosive simulation, Stress wave measurement, Transmitted waves.*

1. Introduction

When explosives are detonated, the high-pressure blast products exert intense forces on the walls of the blast holes, causing rock particles to displace. This displacement induces movement in adjacent particles, propagating oscillations through the rock medium, thereby generating stress waves. Since the previous century, numerous scientists have investigated the destructive effects of stress waves on rock formations, culminating in the theory of rock fracturing via stress waves. Researchers such as Khanukaev and Kumao Hino have contributed to this area, asserting that when the intensity of stress waves exceeds the dynamic strength of the material, the material at that location fractures [1, 2]. Consequently, stress waves are pivotal in breaking rock and material structures during blasting operations.

The measurement of stress waves in rock environments has been extensively studied. However, two primary methods dominate this research:

Strain measurement devices: This method involves using strain gauges to record deformations in the rock medium. Stress wave intensity is then calculated based on the stress-strain relationship of the material [3-6].

$$\sigma = E.\varepsilon \qquad (1)$$

where: σ is stress in the material or medium; E is elastic modulus of the material; ε is strain of the material at the measurement point.

While strain measurement devices are useful, they have several limitations. The stress-strain

© 2025 by the authors; licensee Learning Gate
History: Received: 23 December 2024; Revised: 18 February 2025; Accepted: 21 February 2025; Published: 22 March 2025
* Correspondence: ducnt1988@lqdtu.edu.vn

relationship according to Equation 1 is mainly valid under static or slowly varying loads. For high-speed dynamic loads, such as those caused by blasts or impacts, both the elastic modulus and the material strength can change significantly [7, 8]. Moreover, this relationship becomes unsuitable in the plastic state of the material, leading to inaccuracies in determining the complete parameters of the stress waves. Additionally, the insertion of strain gauges into the rock medium can disrupt its initial homogeneity, introducing further errors.

Method 2: A second approach to measure blast-induced stress waves in rock involves using voltage-based pressure sensors submerged in water. In this method, a water pit with dimensions L×B×H=4m×4m×3m and vertical walls is created along the wave propagation path. The sensors are placed close to the pit walls, approximately 2–8 mm from the surface, opposite to the blast charges positioned within the rock at a specific distance from the wall. The sensors record the intensity of transmitted waves. The incident stress wave intensity in the rock is then determined using the sensor readings and a transmitted coefficient [9].

$$\sigma = \frac{p_n}{T_{12}} \tag{2}$$

where: p_n is the pressure value of the wave transmitted in the water environment measured by the sensor, T_{12} is transmitted coefficient of stress waves;

Although water pits of the specified dimensions offer a means of measuring stress waves, their setup can be impractical and costly. For small-scale blasts or experiments on small rock samples, such pits are infeasible.

Alternative methods have been proposed, including using accelerometers, displacement sensors, and velocity sensors to measure rock displacement caused by blasts [10-12]. However, these sensors are typically surface-mounted and cannot be embedded within the rock medium. Consequently, they only measure displacement parameters, not the intensity of stress waves.

Numerical simulations are another approach employed by researchers to model the effects of blasts and assess their impact on rock formations [13-15]. This method provides a comprehensive analysis of blast impacts, including the stress wave field at any point within the rock. It is cost-effective compared to physical experiments. However, the material models used in simulations often fail to fully capture the complex behaviors of materials under explosive loads or account for natural factors influencing blast outcomes. As a result, the simulation results tend to deviate significantly from experimental observations.

Proposed method: Based on the analysis of existing measurement methods, particularly Method 2, the authors propose replacing the large water pit with a small, water-filled borehole to house the pressure sensors. This approach reduces costs and labor while enabling easier implementation across various blast scales, especially for small-scale experiments on limited rock samples. The proposed borehole diameter is 14 mm, chosen to match the specifications of the PCB-W138-A05 water pressure sensor manufactured by Piezoelectric, USA.

However, in using a circular borehole, the transmitted stress wave intensity from rock to water is influenced by the curved contact surface. The formular 3, applicable for flat interfaces, require modification to account for the shape of the borehole. Therefore, an additional correction factor must be incorporated to adjust for the borehole's geometry when calculating stress in the rock medium.

2. Materials and Methods

2.1. Fundamentals of Stress Wave Transmission Across Interfaces

When a stress wave propagates to the interface between two media at an angle of incidence α_{I1}, it generates reflected waves (reflected P-wave and reflected S-wave) and transmitted waves (transmitted P-wave and transmitted S-wave) with respective angles of reflection and transmission α_{R1}, β_{R1}, α_{T2}, β_{T2} Figure. 1.

Edelweiss Applied Science and Technology
ISSN: 2576-8484
Vol. 9, No. 3: 1692-1704, 2025
DOI: 10.55214/25768484.v9i3.5680
© 2025 by the authors; licensee Learning Gate

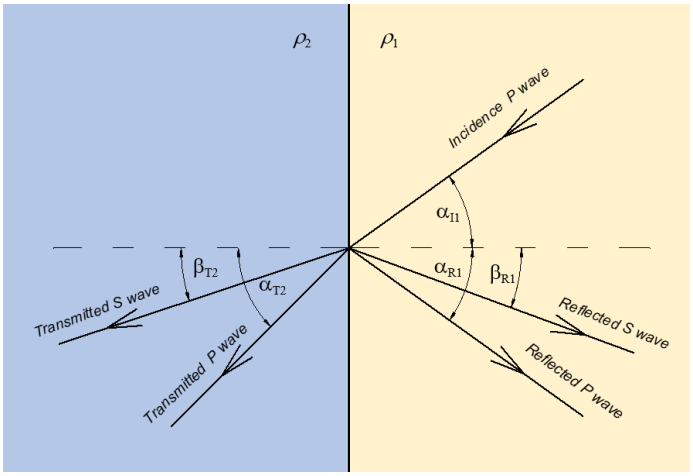

Figure 1.
Reflection and transmittion of stress wave at the interface.

According to Snell's law, consistent with Huygens' principle, the following relationship holds:

$$\frac{\sin\alpha_{I1}}{c_{L1}}=\frac{\sin\alpha_{R1}}{c_{L1}}=\frac{\sin\beta_{R1}}{c_{S1}}=\frac{\sin\alpha_{T2}}{c_{L2}}=\frac{\sin\beta_{T2}}{c_{S2}} \quad (3)$$

In the case of a P-wave incident perpendicularly to the free surface ($\alpha_{I1}=0$), all angles α_{R1}, β_{R1}, α_{T2}, β_{T2}, are zero. Consequently, only two waves are generated: the reflected P-wave and the transmitted P-wave. Based on the continuity assumptions for displacement at the interface, the equations for particle velocity and stress at the interface are given as [16, 17].

$$\upsilon_{I1}+\upsilon_{R1}=\upsilon_{T1} \quad (4a)$$

$$\sigma_{I1}+\sigma_{R1}=\sigma_{T1} \quad (4b)$$

where: $\sigma_{I1};\sigma_{R1};\sigma_{T1}$ are particle velocities of the incident, reflected, and transmitted waves at the interface, respectively; $\upsilon_{I1};\upsilon_{R1};\upsilon_{T1}$ are stresses of the incident, reflected, and transmitted waves at the interface, respectively.

Furthermore, solving the stress wave propagation equation in solids: $\rho\frac{\partial^2 u}{\partial t^2}=E\frac{\partial^2 u}{\partial x^2}$

and applying Hooke's law yields the relationship between stress and particle velocity [15]: $\sigma=\pm\rho c_L\upsilon$. The negative sign indicates a wave propagating in the positive x-direction, while the positive sign represents a wave propagating in the negative x-direction.

Therefore

$$\sigma_{I1}=-\rho_1 c_{L1}\upsilon_{I1} \quad (5a)$$

$$\sigma_{T1}=-\rho_2 c_{L2}\upsilon_{T1} \quad (5b)$$

$$\sigma_{R1}=\rho_1 c_{L1}\upsilon_{T1} \quad (5c)$$

Edelweiss Applied Science and Technology
ISSN: 2576-8484
Vol. 9, No. 3: 1692-1704, 2025
DOI: 10.55214/25768484.v9i3.5680
© 2025 by the authors; licensee Learning Gate

Substituting Equation (5) into Equation (4a) gives $\frac{-\sigma_{I1}}{\rho_1 c_{L1}} + \frac{\sigma_{R1}}{\rho_1 c_{L1}} = \frac{-\sigma_{T1}}{\rho_2 c_{L2}}$ (6)

By solving Equations (4b) and (6), we obtain:

$$\sigma_{R1} = \frac{\rho_2 c_{L2} - \rho_1 c_{L1}}{\rho_1 c_{L1} + \rho_2 c_{L2}} \sigma_{I1} \tag{7a}$$

$$\sigma_{T1} = \frac{2\rho_2 c_{L2}}{\rho_1 c_{L1} + \rho_2 c_{L2}} \sigma_{I1} \tag{7b}$$

Substituting Equations (5c) and (5a) into both sides of Equation (7a) and substituting Equations (5a) and (5b) into Equation (7b) yields:

$$\upsilon_{R1} = -\left(\frac{\rho_2 c_{L2} - \rho_1 c_{L1}}{\rho_1 c_{L1} + \rho_2 c_{L2}} \right) \upsilon_{I1} \tag{8a}$$

$$\upsilon_{T1} = \frac{\rho_1 c_{L1}}{\rho_2 c_{L2}} \left(\frac{2\rho_2 c_{L2}}{\rho_1 c_{L1} + \rho_2 c_{L2}} \right) \upsilon_{I1} \tag{8b}$$

Let: $\xi_{12} = \frac{\rho_1 c_1}{\rho_2 c_2}$; $R_{12} = \frac{1 - \xi_{12}}{1 + \xi_{12}}$ and $T_{12} = \frac{2}{1 + \xi_{12}}$

$$\Rightarrow \begin{cases} \sigma_{R1} = R_{12}\sigma_{I1} \\ \sigma_{T1} = T_{12}\sigma_{I1} \\ \upsilon_{R1} = -R_{12}\upsilon_{I1} \\ \upsilon_{T1} = \xi_{12} T_{12} \upsilon_{I1} \end{cases}$$

where: R_{12} is the stress wave reflection coefficient; T_{12} is the stress wave transmission coefficient; ξ_{12} is the ratio of the acoustic impedance of the two media.

Thus, the parameters of the incident and reflected stress waves can be fully determined based on the transmitted stress wave, given the reflection and transmission coefficients when the stress wave propagates through two media.

2.2. Simulation Study

2.2.1. Research Model Description

The study model comprises a concrete block of strength grade B22.5 with dimensions L×B×H=1.5×0.8×0.5 m. The block contains two drilled holes: one with a diameter of 27 mm for explosive placement and the other with a diameter of 14 mm, filled with water. The concrete block is placed in contact with water.

A steel tube with an outer diameter of 27 mm and a wall thickness of 1.5 mm is affixed to the wall of the explosive-containing hole (Figure 2). Inside this hole, a cylindrical charge of TNT weighing 1.0 g is placed, with dimensions r=6 mm and h=30 mm.

Edelweiss Applied Science and Technology
ISSN: 2576-8484
Vol. 9, No. 3: 1692-1704, 2025
DOI: 10.55214/25768484.v9i3.5680
© 2025 by the authors; licensee Learning Gate

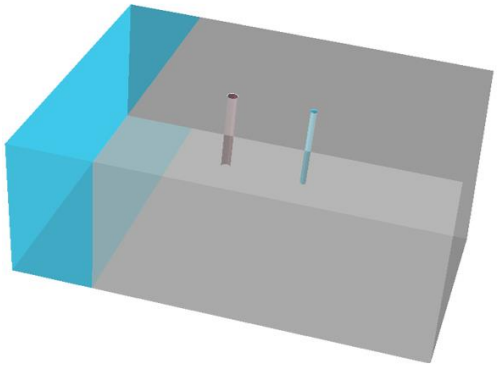

Figure 1.
Simulation Model.

2.2.2. Material Models

Concrete: The Holmquist-Johnson-Cook (HJC) model, designed for brittle materials subjected to high-rate loading such as impacts or explosions, is employed to model the B22.5 concrete. The HJC model parameters for B22.5 concrete are derived based on the study by Ren, et al. [16].

Water: The Grüneisen equation of state (EoS) is used to model water. The parameters for water under the Grüneisen EoS are adopted from the research by Hinrichsen, et al. [17] Alia and Souli [18].

TNT Explosive: The Jones-Wilkins-Lee (JWL) equation of state has been applied by many authors to model TNT explosives. The TNT parameters follow the publication by Alia and Souli [18].

Steel: The Continuum Damage Mechanics (CDM) model is used to simulate steel material behavior. The steel parameters are based on the findings of Kumar, et al. [19].

Edelweiss Applied Science and Technology
ISSN: 2576-8484
Vol. 9, No. 3: 1692-1704, 2025
DOI: 10.55214/25768484.v9i3.5680
© 2025 by the authors; licensee Learning Gate

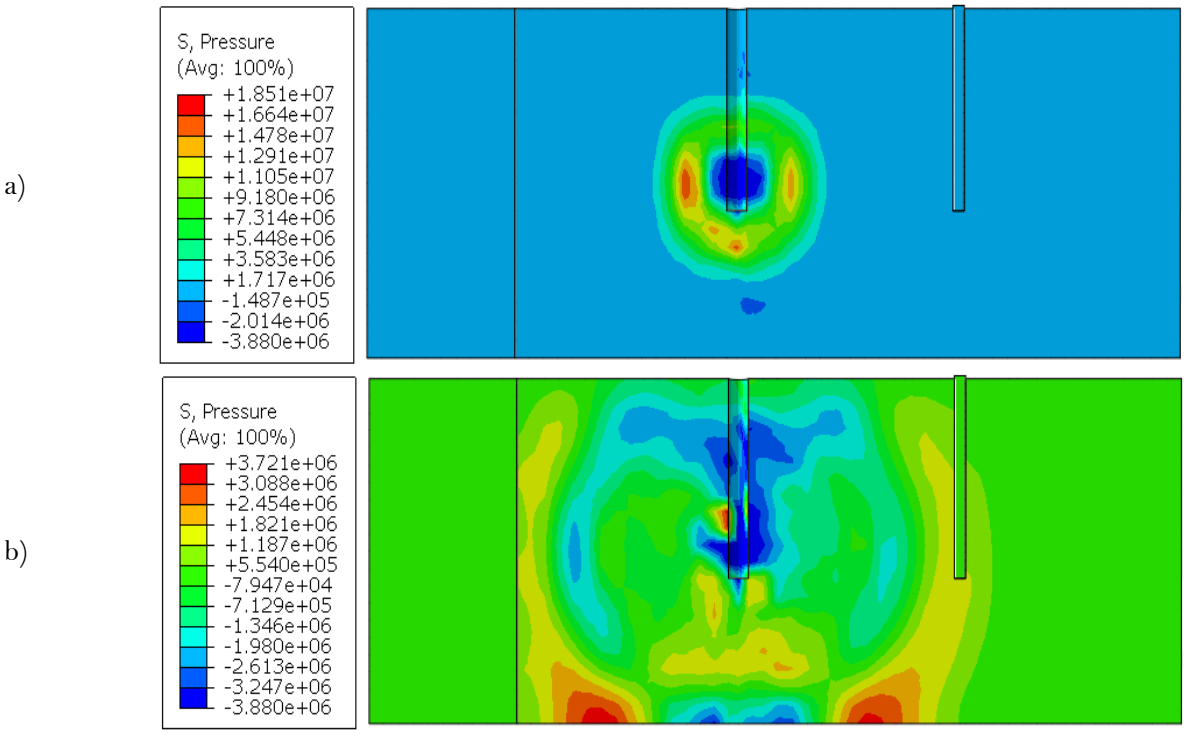

Figure 2.
Formation and propagation of stress waves during explosion.

2.2.3. Simulation Results

a- blasting stress wave formed after detonation of explosive charge; b- blasting stress wave propagates to water medium at interface and in borehole

As the stress waves propagate to the interface between the two media, they transmitte from the concrete into the water, generating stresses within the water medium.

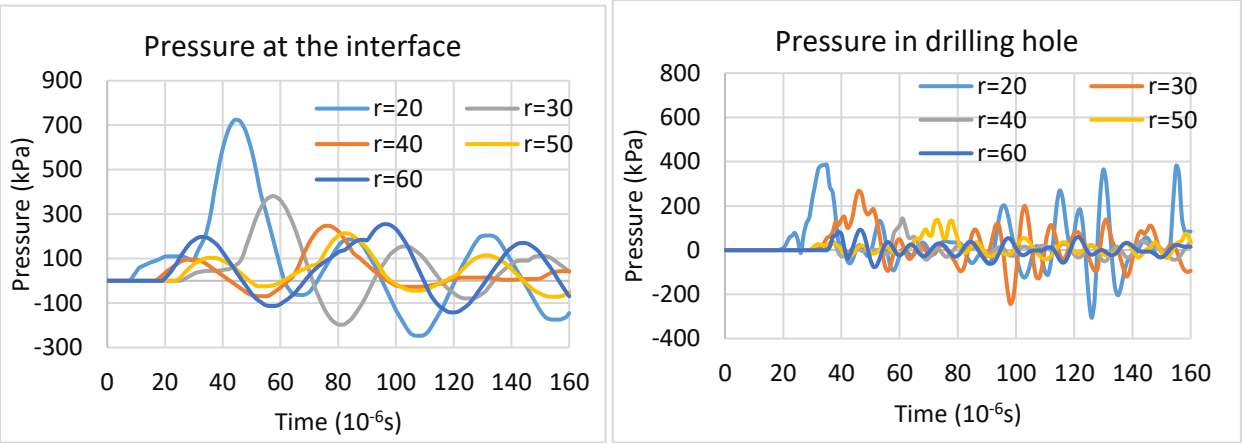

Figure 3.
Stress waves profiles over time.

From the plots shown in Figure 4, it can be observed that the maximum pressure of the transmitted wave at the interface exceeds the corresponding pressure value within the water-filled borehole. To evaluate this disparity, it is necessary to compile the maximum values of the refracted wave pressures at

Edelweiss Applied Science and Technology
ISSN: 2576-8484
Vol. 9, No. 3: 1692-1704, 2025
DOI: 10.55214/25768484.v9i3.5680
© 2025 by the authors; licensee Learning Gate

various distances. By extracting the maximum pressure values of the stress waves at different distances from the charge's center to the interface and to the borehole, the results are summarized in **Table 1**.

Table 1.
Transmitted wave pressure peak results from simulation study.

Distance r (cm)	Maximum pressure	
	at the interface (si)	in the drilling hole (si)
20	724041	384456
30	380337	268721
40	247302	143774
50	213526	137458
60	196913	88985.7

From the results in Table 1, the maximum pressure values of the transmitted waves are plotted, yielding the points shown in Figure 5.

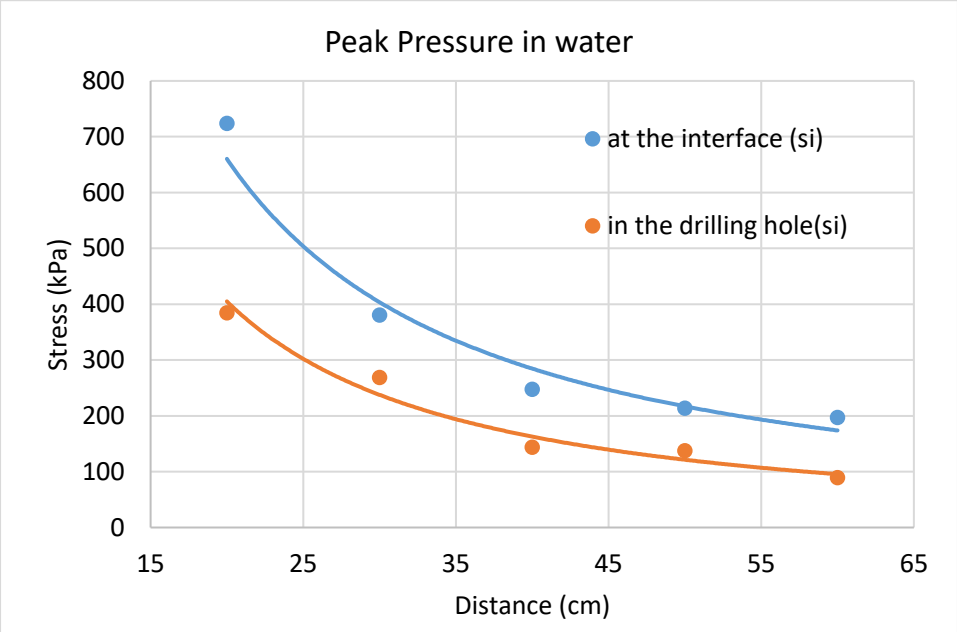

Figure 4.
Peak pressure of measuring points in water at the interface and borehole according to distance to the explosion centre.

2.3. Experimental Study

2.3.1. Experimental Set Up:

The pressure of the explosion waves was measured in a water-filled borehole along the wave propagation path. The experimental model consisted of a coral concrete block with dimensions L×B×H=1.8×0.8×0.5 m. The block was drilled with two types of boreholes: one with a diameter d=27 mm for explosive placement and others with a diameter d=14 mm filled with water to house water pressure sensors. The concrete block's surface was in contact with water. The distances from the explosive charge to the interface and the water-filled boreholes (d=14 mm) were r=20, 30, 40, 50, and 60 cm, respectively Figure 6.

2.3.2. Experimental Materials

Concrete: The concrete used had a compressive strength equivalent to grade B22.5. Its mix

Edelweiss Applied Science and Technology
ISSN: 2576-8484
Vol. 9, No. 3: 1692-1704, 2025
DOI: 10.55214/25768484.v9i3.5680
© 2025 by the authors; licensee Learning Gate

proportions were based on the research of Duong, et al. [20].

Explosive Material: The explosive charge, manufactured by Z121 Factory, was equivalent to a cylindrical TNT charge weighing 1.0 g, with dimensions d=6 mm and h=45 mm. The charge was placed at a depth of h=25 cm.

2.3.3. Measurement Equipment

Pressure Sensors: W138-A05 water pressure sensors (PCB brand) were used to measure the pressure of refracted waves transitioning from concrete to water. The sensors were placed in water-filled boreholes at distances of 20, 30, 40, 50, and 60 cm from the explosion center.

Data Acquisition System: An NI SCXI-1000DC multi-channel dynamic data acquisition system was used to record signals from the sensors Figure 7.

Explosive detonations were conducted, and stress wave measurements were taken at the borehole locations for the specified distances. Each distance was tested 3–4 times to ensure data reliability.

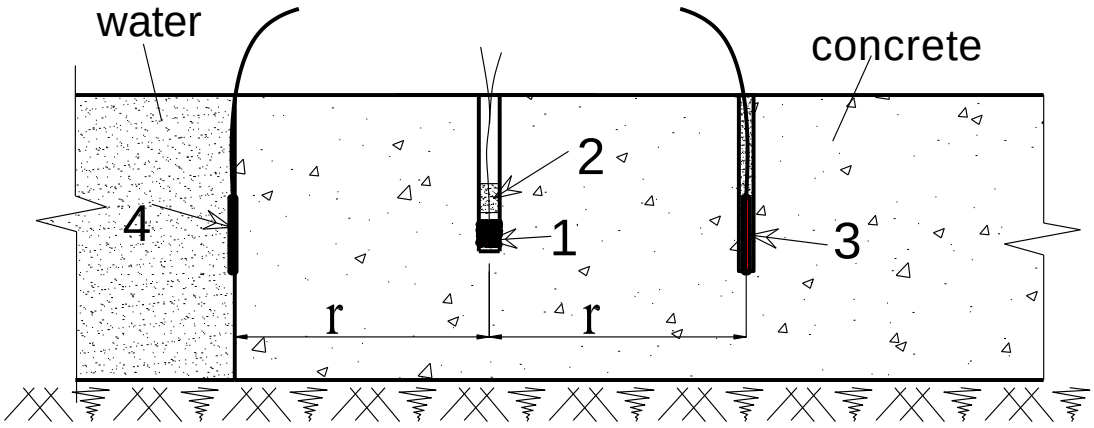

Figure 6.
Experimental layout diagram.

1- Explosive charge; 2- Steaming; 3- Sensor placed in borehole; 4- Sensor at interface

Figure 7.
Measurement equipment.

Edelweiss Applied Science and Technology
ISSN: 2576-8484
Vol. 9, No. 3: 1692-1704, 2025
DOI: 10.55214/25768484.v9i3.5680
© 2025 by the authors; licensee Learning Gate

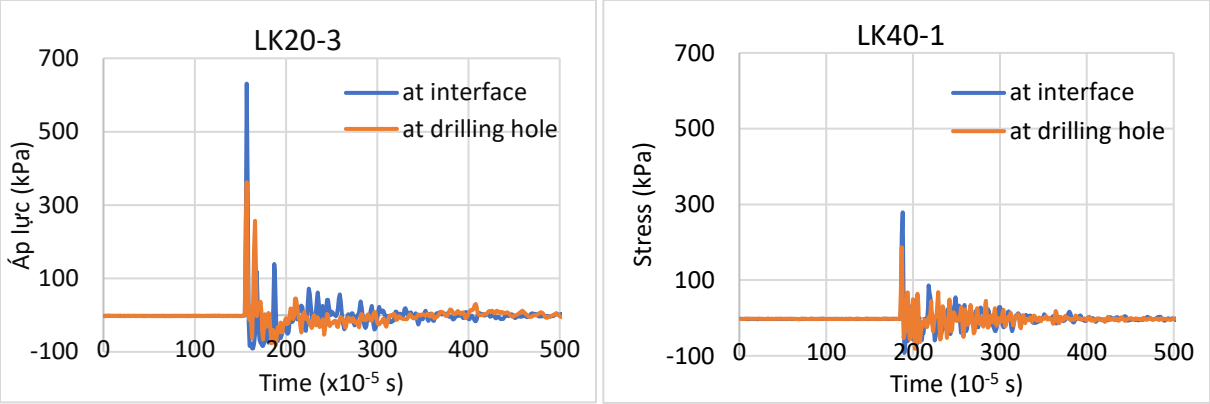

Figure 8.
Transmitted wave pressure over time.

2.3.4. Experimental Results

The stress wave (transmitted wave) pressure profiles over time in the water-filled boreholes are shown in Figure . The profiles clearly indicate distinct compression and tension phases, with the compression phase exhibiting a much higher intensity than the tension phase.

The maximum measured intensity of the transmitted wave at the interface consistently exceeded the values recorded in the water-filled boreholes. The results of maximum stress intensities for each measurement distance are presented in Table 2.

Table 2.
Maximum stress values at measure.

Label	Distance r (cm)	Measurement Number	Maximum Pressure	
			At the interface	In drilling hole
LK20-1	20	1	479.91	368.24
LK20-2	20	2	613.192	370.8869
LK20-3	20	3	631	362
LK20-4	20	4	590.4078	409.4039
LK30-1	30	1	368.4425	181.3285
LK30-2	30	2	404.3092	215.9789
LK30-3	30	3	480.5455	256.1552
LK30-4	30	4	509.285	222.734
LK40-1	40	1	279.1833	187.0356
LK40-2	40	2	247.7999	167.4683
LK40-3	40	3	246.5529	181.7726
LK40-4	40	4	243.6993	178.512
LK50-1	50	1	172.6021	102.2439
LK50-2	50	2	196.8529	115.4926
LK50-3	50	3	214.99	138.9326
LK60-1	60	1	179	101
LK60-2	60	2	177.493	82.06508
LK60-3	60	3	151.6119	83.28804
LK60-4	60	4	202.56	93.48

Edelweiss Applied Science and Technology
ISSN: 2576-8484
Vol. 9, No. 3: 1692-1704, 2025
DOI: 10.55214/25768484.v9i3.5680
© 2025 by the authors; licensee Learning Gate

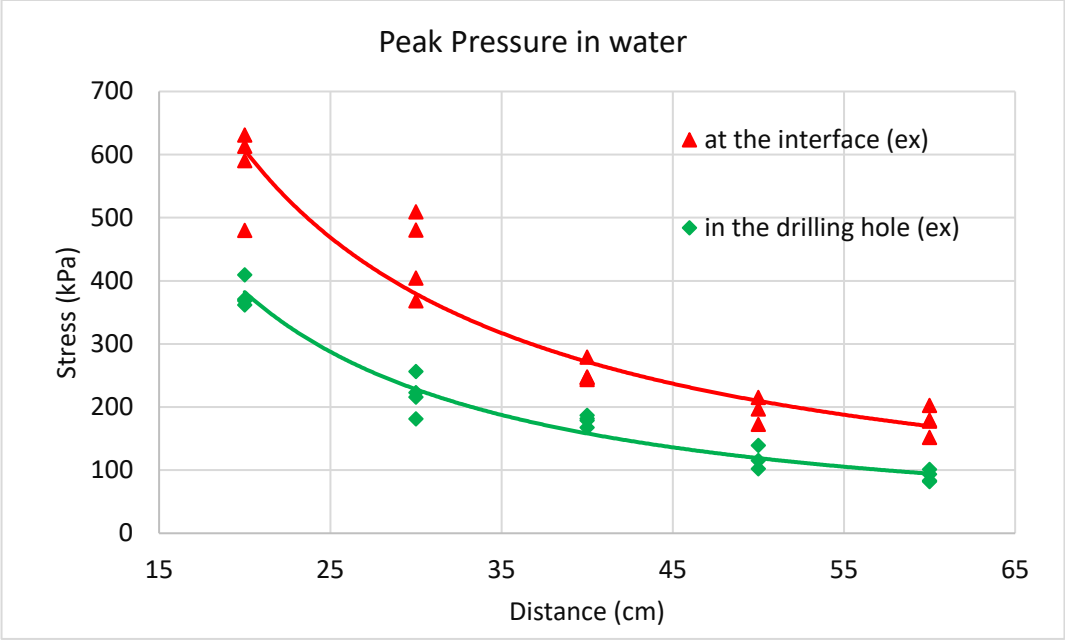

Figure 5.
Peak Stress Wave Measured at the Interface and in the Borehole.

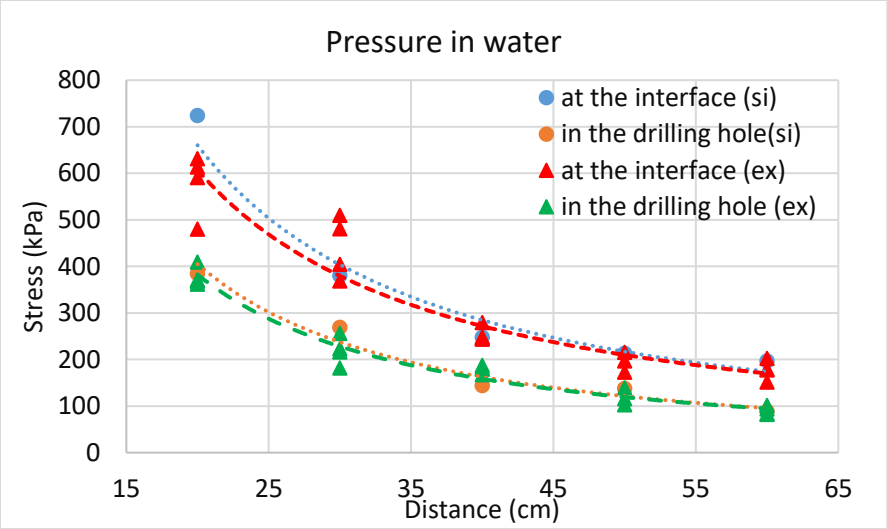

Figure 6.
Comparison of Simulation and Experiment.

3. Results and Discussion

The attenuation behavior of transmitted waves during propagation, as obtained from simulations and experimental studies, is illustrated in Figure 10 It is evident that the results from the simulation and experimental methods are closely aligned.

Figure 11 depicts the correlation between the maximum intensities of refracted waves measured at the interface and in the borehole, based on both simulation and experimental data. The correlation behavior between the stress wave intensities at the two measurement locations can be expressed as follows:

Edelweiss Applied Science and Technology
ISSN: 2576-8484
Vol. 9, No. 3: 1692-1704, 2025
DOI: 10.55214/25768484.v9i3.5680
© 2025 by the authors; licensee Learning Gate

From simulation: $P_{interface}=0.568P_{borehole}$;
From experiment: $P_{interface}=0.598P_{borehole}$;
where: $P_{borehole}$: Maximum pressure of the refracted wave in the borehole;
$P_{interface}$: Maximum pressure of the refracted wave at the interface.

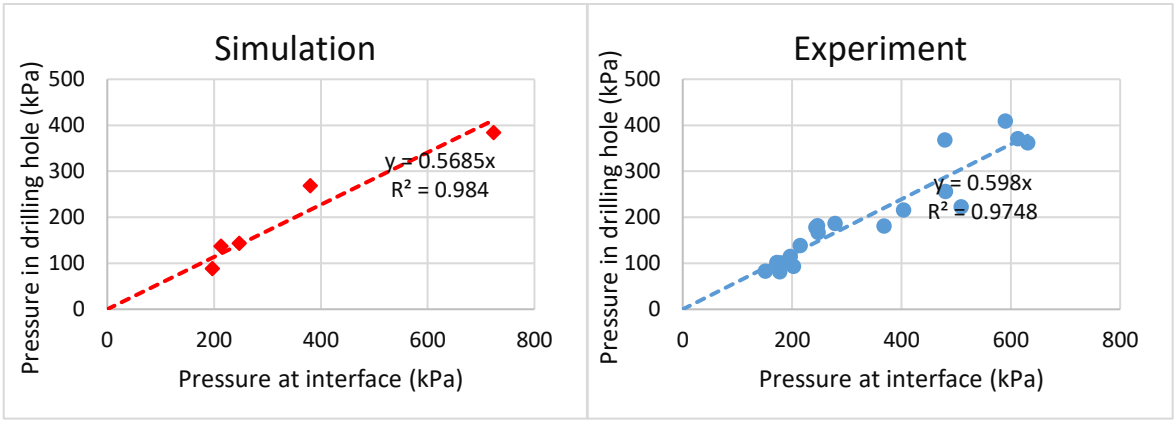

Figure 7.
Correlation of maximum intensities of transmitted waves at two measurement locations.

The proportional coefficient between the stress at the interface and in the borehole, derived from simulation data, is 0.568, while that obtained from experimental data is 0.598. This coefficient represents the influence of borehole geometry compared to a planar surface when refracted stress waves propagate into the water medium.

The error between the experimental and simulation methods is small (approximately 5%), demonstrating the validity of the research model. The consistency between experimental and simulation results confirms the accuracy and reliability of using water pressure sensors in boreholes to measure stress waves in rock and soil media.

4. Conclusion

This study has addressed the challenge of accurately measuring blasting-induced stress waves in water-filled boreholes, particularly in the context of small-scale blasting scenarios. Conventional methods involving large water pits, while effective, are impractical for smaller experiments or rock samples. By proposing and validating an alternative measurement method using water pressure sensors in small-diameter boreholes, this research offers a cost-effective and scalable solution for analyzing stress wave intensity in hard rock formations.

Through a combination of numerical simulations and controlled experiments, the study successfully determined a conversion coefficient of 0.598 for translating borehole measurement data into equivalent values for water-filled pits. This coefficient, derived from empirical and computational results, accounts for the influence of borehole geometry on wave refraction dynamics. The close alignment between the experimental and simulation outcomes, with an error margin of approximately 5%, underscores the reliability of the proposed method and the robustness of the research approach.
Key findings include:

Validation of the Borehole Method: The study demonstrated that water pressure sensors placed in 14-mm boreholes could reliably measure refracted stress waves, providing results comparable to those obtained using larger water-filled pits.

Conversion Coefficient Determination: The experimentally derived coefficient of 0.598 and the simulation-based coefficient of 0.568 indicate consistent correlations between the stress wave intensity at

Edelweiss Applied Science and Technology
ISSN: 2576-8484
Vol. 9, No. 3: 1692-1704, 2025
DOI: 10.55214/25768484.v9i3.5680
© 2025 by the authors; licensee Learning Gate

the borehole and the interface.

Practical Benefits: The proposed method significantly reduces the cost, labor, and complexity associated with constructing large water pits, making it particularly advantageous for small-scale experiments.

Furthermore, this research contributes to the broader understanding of stress wave propagation in heterogeneous media, providing insights into the attenuation and refraction behaviors of stress waves at interfaces. The adoption of advanced material models such as the Holmquist-Johnson-Cook (HJC) for concrete, the Grüneisen equation for water, and the JWL equation for TNT enhanced the precision of the simulations, enabling a detailed evaluation of wave dynamics.

In conclusion, the innovative approach presented in this study offers a practical, scalable, and accurate solution for measuring blasting-induced stress waves in rock media. It bridges the gap between large-scale experimental setups and the need for cost-efficient methods in small-scale studies, paving the way for more accessible and precise investigations into the mechanics of blasting in geological environments.

Funding:
This study received no specific financial support.

Institutional Review Board Statement:
Not applicable.

Transparency:
The authors confirm that the manuscript is an honest, accurate and transparent account of the study that no vital features of the study have been omitted and that any discrepancies from the study as planned have been explained. This study followed all ethical practices during writing.

Competing Interests:
The authors declare that they have no competing interests.

Authors' Contributions:
All authors contributed equally to the conception and design of the study. All authors have read and agreed to the published version of the manuscript.

Acknowledgements:
The authors would like to thank the Le Quy Don Technical University for giving me the opportunity to conduct this research.

Copyright:
© 2024 by the authors. This article is an open access article distributed under the terms and conditions of the Creative Commons Attribution (CC BY) license (https://creativecommons.org/licenses/by/4.0/).

References
[1] H. S. Giao, D. T. Thang, L. V. Quyen, and H. T. Trung, *Chemical explosions - theory and practice*. Ha Noi: Science and Technology Publishing House, 2010.

[2] D. T. Thang, B. X. Nam, and T. Q. Hieu, *Blasting in mining and construction*. Ha Noi: Publishing House of Natural Science and Technology, 2015.

[3] L. Y. Chi, Z.-X. Zhang, A. Aalberg, J. Yang, and C. C. Li, "Measurement of shock pressure and shock-wave attenuation near a blast hole in rock," *International Journal of Impact Engineering*, vol. 125, pp. 27-38, 2019. https://doi.org/10.1016/j.ijimpeng.2018.11.002

[4] X. Huo, X. Qiu, X. Shi, H. Chen, C. Zong, and C. Xie, "Attenuation characteristics of blasting stress under decoupled cylindrical charge," *Rock Mechanics and Rock Engineering*, vol. 56, no. 6, pp. 4185-4209, 2023. https://doi.org/10.1007/s00603-023-03286-3

[5] X. Shi, Z. Zhang, X. Qiu, and Z. Luo, "Experiment study of stemming length and stemming material impact on rock fragmentation and dynamic strain," *Sustainability*, vol. 15, no. 17, p. 13024, 2023. https://doi.org/10.3390/su151713024

[6] E. O. Mnndeli, N. F. Kusov, A. A. Sorneev, G. I. Martsinkevich, and Mnndeli, *Study of stress waves during explosion in rocks*. Moscow: Nauka, 1978.

[7] L. J. Malvar and J. E. Crawford, "Dynamic increase factors for concrete," in *Proceedings of the Twenty-Eighth DoD Explosives Safety Seminar, Orlando*, 1998.

[8] N. Q. Trung and V. T. Tung, *Explosive*. Ha Noi: Le Quy Don Technical University, 2005.

[9] K. Fuławka, P. Mertuszka, M. Szumny, L. Stolecki, and K. Szczerbiński, "Application of MEMS-based accelerometers for near-field monitoring of blasting-induced seismicity," *Minerals*, vol. 12, no. 5, p. 533, 2022. https://doi.org/10.3390/min12050533

[10] B. Jayasinghe, Z. Zhao, A. G. T. Chee, H. Zhou, and Y. Gui, "Attenuation of rock blasting induced ground vibration in rock-soil interface," *Journal of Rock Mechanics and Geotechnical Engineering*, vol. 11, no. 4, pp. 770-778, 2019. https://doi.org/10.1016/j.jrmge.2018.12.009

[11] K. Kong, "Blasting vibration assessment of rock slopes and a case study," in *Slope Stability 2013: Proceedings of the 2013 International Symposium on Slope Stability in Open Pit Mining and Civil Engineering*, 2013: Australian Centre for Geomechanics, pp. 1335-1344.

[12] M. D. Banadaki and B. Mohanty, "Numerical simulation of stress wave induced fractures in rock," *International Journal of Impact Engineering*, vol. 40, pp. 16-25, 2012. https://doi.org/10.1016/j.ijimpeng.2011.08.010

[13] X. Ding, Y. Yang, W. Zhou, W. An, J. Li, and M. Ebelia, "The law of blast stress wave propagation and fracture development in soft and hard composite rock," *Scientific Reports*, vol. 12, no. 1, p. 17120, 2022. https://doi.org/10.1038/s41598-022-22109-z

[14] D. T. Thang, N. T. Duc, and N. N. Thuy, "Research on the attenuation of blasting stress wave while propagation in limestone," *Journal of Construction*, vol. 11, pp. 70-75, 2023.

[15] Z.-X. Zhang, *Rock fracture and blasting: Theory and applications*. Oxford, UK: Butterworth-Heinemann, 2016.

[16] G.-M. Ren, H. Wu, Q. Fang, and X.-Z. Kong, "Parameters of Holmquist–Johnson–Cook model for high-strength concrete-like materials under projectile impact," *International Journal of Protective Structures*, vol. 8, no. 3, pp. 352-367, 2017. https://doi.org/10.1177/2041419617721552

[17] R. Hinrichsen, M. Moshier, and A. Kurtz, "High velocity impacts of man portable air defense systems (MANPADS) on selected targets," in *45th AIAA/ASME/ASCE/AHS/ASC Structures, Structural Dynamics & Materials Conference*, 2004, p. 1917.

[18] A. Alia and M. Souli, "High explosive simulation using multi-material formulations," *Applied Thermal Engineering*, vol. 26, no. 10, pp. 1032-1042, 2006. https://doi.org/10.1016/j.applthermaleng.2005.10.018

[19] M. Kumar, U. Deep, and P. Dixt, "Simulation and analysis of ballistic impact using continuum damage mechanics (CDM) model," *Procedia Engineering*, vol. 173, pp. 190-197, 2017. https://doi.org/10.1016/j.proeng.2016.12.057

[20] L. H. Duong, T. V. Cuong, N. T. Ta, D. Q. Trung, and N. X. Bang, "Design of coral concrete mixtures," *Journal of Construction*, vol. 3, pp. 72-77, 2024.

Edelweiss Applied Science and Technology
ISSN: 2576-8484
Vol. 9, No. 3: 1692-1704, 2025
DOI: 10.55214/25768484.v9i3.5680
© 2025 by the authors; licensee Learning Gate